17th Brazilian Congress of Thermal Sciences and Engineering
November 25th-28th, 2018, Águas de Lindóia, SP, Brazil

# ENCIT-2018-0432
# LOW COST THRUST VECTORING CONTROL SYSTEM FOR A SOLID PROPELLANT ROCKET

**Daniel Resemini**
**Fernando de Souza Costa**
National Institute for Space Research, Rod. Pres. Dutra, km 40, Cachoeira Paulista, SP, Brazil
danielresemini@hotmail.com, fernando.costa@inpe.br

***Abstract.*** *A thrust vectoring control system with a solid propellant rocket motor was designed using two airfoils adjacent to the nozzle exit. The components and the integration of the thrust vector control system were analysed. The control software and the hardware were based on Arduino platform, and a Kalman filter was used to reduce noise of the input data from the inertial measurement unit. Experimental data were obtained, including chamber pressure and thrust, and were compared to the results of a simplified mathematical model. The results indicate the feasibility of a low cost off the shelf and efficient thrust vectoring control system for rockets with low to moderate accelerations.*

***Keywords:*** *Rocket propulsion, Thrust vectoring control, Arduino, Potassium nitrate.*

## 1. INTRODUCTION

The last decade has been marked by major advances in aerospace engineering, particularly with regard to the reuse of launch vehicles. The possibility of not having to discard a rocket after its use greatly reduces the cost per launch and, this way, turns the space into a more accessible market for several enterprises, since the launch of satellites, asteroid mining, and even space tourism or colonization (Schaefermeyer, 2011). A thrust vectoring control mechanism consists of a feedback system where the dynamics of the body where the sensor is installed is measured through accelerometers and gyroscopes having this data reinserted as the system's input allowing new calculations to be made by an embedded computer.

There are lots of established products in industry that use thrust vectoring control, what is the case of many known missiles that a few countries developed decades ago. Despite this, the research on these mechanisms should be done continuously in order to master and improve, as much as possible, such a strategic technology.

The present work aims to contribute with the diffusion of the basic knowledge involved in a thrust vectoring control system, in particular an analysis of each system component and the integration of the complete system. A thrust vectoring control system for a solid propellant rocket motor was designed, built and tested. Experimental data were obtained showing the feasibility of a low cost off the shelf and efficient vectoring control system for rockets with low to moderate accelerations.

## 2. METHODOLOGY

An embedded computer must be precisely programmed with the information of all other rocket subsystems, such as airfoil aerodynamics characteristics, thermodynamic properties of the exhaust gases and mechanical characteristics of the body, such as mass and moment of inertia, in order to have a good performance of the thrust vectoring control.

Figure 1 shows a scheme of the thrust vector control system designed, comprising a rocket chamber with a nozzle, two airfoils adjacent to the nozzle exit and the embedded electronics (accelerometer, gyroscope, microcontroller and servomotor). The system is attached to a pendulum to evaluate the control mechanism.

Figure 1. Thrust vectoring control experiment

### 2.1 Thrust vectoring control mathematical modeling

In order to control the thrust vector, the exhaust gases are deviated by the airfoils tilting the thrust which produces a torque that changes the angular momentum of the rocket.

The thrust vectoring control system can be described by the following relation, adapted from Tewari (2011):

$$I\ddot{\theta} + \mu\dot{\theta} + (\sum m_i r_i) g\theta = L r_{tvc} \tag{1}$$

where $\theta$ is the angular position, $I$ is the moment of inertia, $L$ is the lift force, μ is the damping coefficient, $r_i$ is the distance of mass $m_i$ to the pendulum rotation axis. The resulting torque, $\tau = I\ddot{\theta}$, acting on the rocket body, is composed by the torque generated by $L$, the damping torque $\mu\dot{\theta}$ and the gravity torque.

The lift force may be obtained through the airfoil lift coefficient as

$$L = C_L \frac{\rho_\infty {u_\infty}^2}{2} S \tag{2}$$

where $S$ is the planar area of the airfoil and $C_L$ is the lift coefficient which can be calculated by

$$C_L = \frac{4\alpha}{\sqrt{M_\infty^2 - 1}} \tag{3}$$

where $\alpha$ is the angle of attack in radians and $M_\infty$ is the Mach number of the flow (Anderson, 2005).

### 2.2 Rocket combustion chamber sizing

To obtain the values of all parameters above described, such as density and Mach number of the exhaust gases, an experiment using a solid propellant rocket was designed.

A rocket motor with a constant burning area was chosen, providing a supersonic flow at the exit of its nozzle and a maximum operating pressure of 10 bar was set. Then, a 0-D transient Matlab code was written and used to evaluate different combinations of chamber diameters and lengths, as well as the grain lengths.

The numerical model first obtains the propellant burn rate for the current chamber pressure:

$$\dot{r}(i) = a P_c(i)^n \tag{4}$$

using the ballistic coefficients *a=0.0029* and *n=0.32* for the 60/40 potassium nitrate/sucrose used (*knsu*).

Then the propellant mass flow rate can be calculated by:

$$\dot{m}_f(i) = \rho_{knsu} S_{burn} \dot{r}(i) \tag{5}$$

where $\rho_{knsu}$ is the propellant density, which is 1860 kg/m$^3$ (Vyverman, 1978), and $S_{burn}$ the propellant burning area.

In order to calculate the mass flow out of the nozzle, it is necessary first to verify if the current chamber pressure is below or above the critical pressure:

$$P_{crit}(i) = \left(\frac{2}{\gamma(i)+1}\right)^{\frac{\gamma(i)}{\gamma(i)-1}} \tag{6}$$

being $\gamma(i)$ the gas specific heat ratio, which varies with chamber temperature and chamber pressure. It is given by a table with data obtained from the CEA NASA (2004) equilibrium code.

For pressures below critical pressure, the discharge coefficient is:

$$\varphi(i) = \left(\frac{P_{atm}}{P_c(i)}\right)^{\frac{1}{\gamma(i)}} \left\{\frac{\gamma(i)}{\gamma(i)-1}\left[1 - \left(\frac{P_{atm}}{P_c(i)}\right)^{\frac{\gamma(i)-1}{\gamma(i)}}\right]\right\}^{\frac{1}{2}} \tag{7}$$

For pressures equal or above the critical pressure the discharge coefficient has its maximum value:

$$\varphi_{max}(i) = \left(\frac{\gamma(i)}{\gamma(i)+1}\right)^{\frac{1}{2}} \left(\frac{2}{\gamma(i)+1}\right)^{\frac{1}{\gamma(i)-1}} \tag{8}$$

Finally it is possible to calculate the nozzle flow rate (Seidel, 1965):

$$\dot{m}_{noz}(i) = P_c(i) A_t \left(\frac{2}{R_c(i) T_c(i)}\right)^{\frac{1}{2}} \varphi(i) \tag{9}$$

The conservation of mass is used to obtain the mass in the combustion chamber for the next step:

$$m_c(i+1) = m_c(i) + m_f(i) - m_{noz}(i) \tag{10}$$

The increment in pressure is obtained by the derivation of the ideal gas equation:

$$dP_c(i+1) = \big(\rho_c(i+1) - \rho_c(i)\big) R_c(i+1) T_c(i+1) + \big(R_c(i+1) - R_c(i)\big) \rho_c(i+1) T_c(i+1) + \\ + \big(T_c(i+1) - T_c(i)\big) \rho_c(i+1) R_c(i+1) \tag{11}$$

being any of the above thermodynamic properties a weighted average between the property in the last step and the same property of the fuel burned. The update in chamber pressure in a step of time *dt* is then calculated:

$$P_c(i+1) = P_c(i) + dP_c(i+1) dt \tag{12}$$

The theoretical results obtained are depicted in the Figures 2 and 3, for the pressure build up phase until steady state is reached, for chamber lengths varying from 10 to 15 cm and propellant grain lengths of 7 cm and 8 cm.

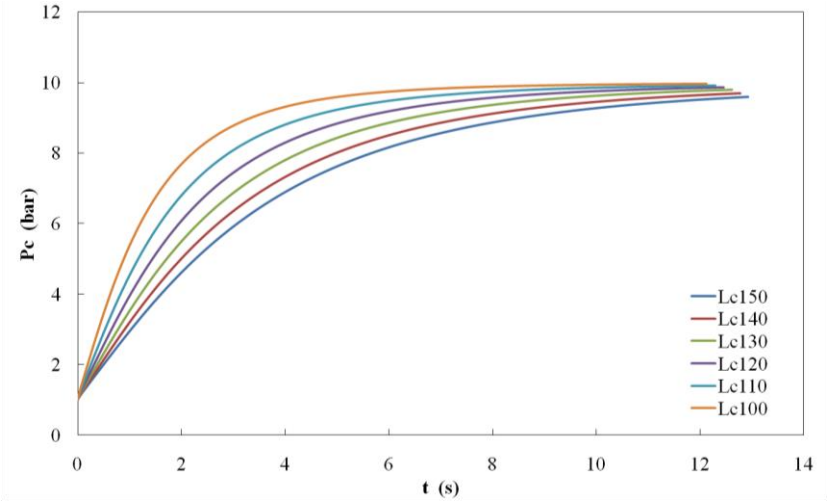


Figure 2. Diagram of chamber pressure ($P_c$) versus burning time for 7 cm grain length.

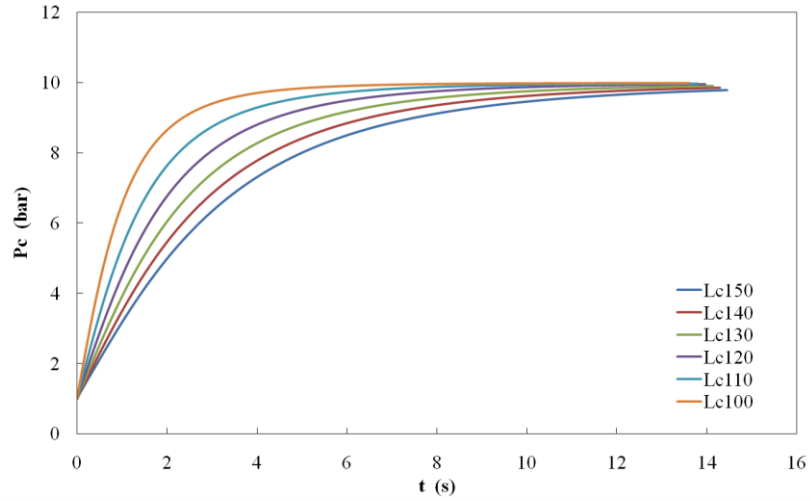


Figure 3. Diagram of chamber pressure ($P_c$) versus burning time for 8 cm grain length.

A chamber diameter of 10.5 cm was defined to yield a maximum chamber pressure of 10 bar for the chosen solid propellant. Considering the lowest build up time, the combustion chamber length of 10 cm with a grain length of 8 cm was defined.

A test bench was designed and built to determine pressure and thrust data through static tests. This experiment was properly instrumented with a load cell and a pressure transducer, as shown in Fig. 4.

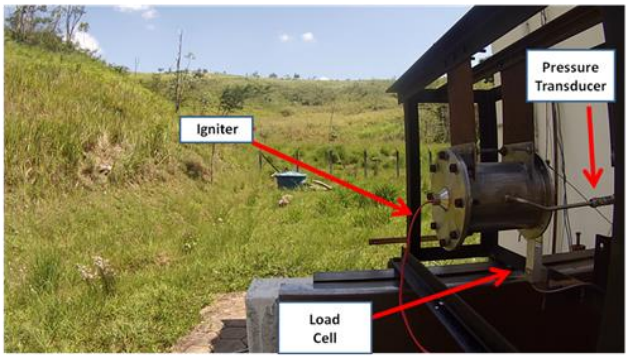


Figure 4. Rocket motor static test assembly

The first static test had as objective to determine an appropriate test procedure as well as to check data acquisition. The motor was loaded with a propellant grain of just 2 cm length, a quarter of the grain length to be used in later tests.

## 3. RESULTS

Several propellant grains of potassium nitrate/sucrose 60/40 were prepared and tested. Pressure and thrust curves obtained in the first static test are shown in Fig. 5.

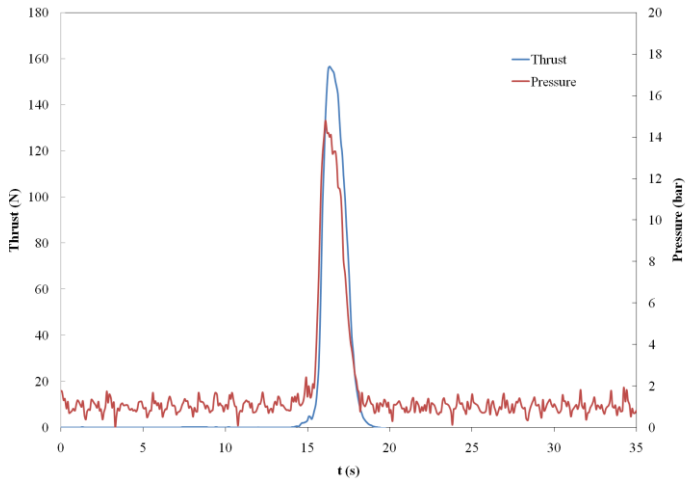


Figure 5. Thrust and Pressure versus time in static fire test 1

Figure 5 indicates that pressures attained higher values than the operational limit set. Further analysis revealed a burning area greater than specified, caused by an inefficient lateral inhibition of the propellant grain. From this result, the processes of casting, molding, inhibiting and enveloping of the propellant grain with epoxy and cardboard, were modified.

After manufacturing of the new properly inhibited grains, tests were performed to verify the grain burning. Figure 6 shows the test of a grain burning in air to verify grain structural integrity, inhibitor behavior and uniformity of burning. This unrestricted burning test took approximately 23 seconds, confirming that the lateral area of the grain remained inhibited during the firing.

Figure 6. Grain burning test in air.

Also, the previous test have shown that the choice for the chamber length of 10 cm could be one of the reasons for noticed combustion instabilities, due to the small specific length. The length of 15 cm was then adopted and further hot fire tests validated the 0-D model for the propulsor, as can be seen in the following Figures 7 and 8.

Figure 7. Hot fire test.

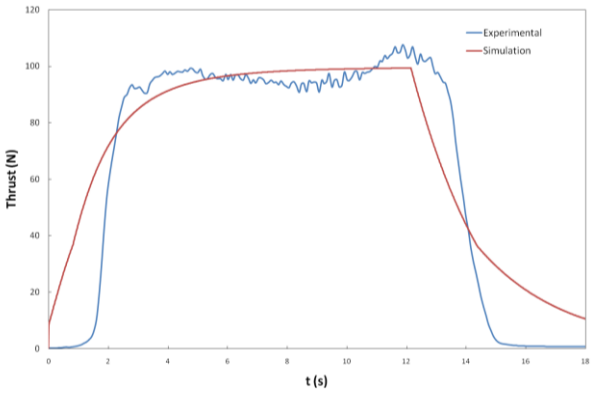


Figure 8. Experimental data from hot fire test versus 0-D simulation data.

It is possible to notice that the experimental thrust curve has an acceptable maximum value if compared to the simulation thrust curve. One of the main difference between the two previous curves is during the build-up phase, when, for simplicity, the model considers that the whole not inhibited area ignites at the same time zero. This implies in a higher mass flowrate during the initial seconds of burning, comparing to the real ignition, which has a delay time to burn the not inhibited area.

Table 1 shows all parameters relevant to the control model:

Table 1. Plant and actuator parameters.

| | Parameters | Initial (Pc = 7bar) | MeOP (Pc = 9.5bar) | Difference (%) |
|---|---|---|---|---|
| Actuador | Area (m2) | 0.00005 | 0.00005 | 0 |
| | raero (m) | 1.210 | 1.210 | 0 |
| | rho (kg/m3) | 0.285 | 0.407 | 42.8 |
| | vel (m/s) | 1197.530 | 1198.390 | 0.1 |
| | Mach | 2.086 | 2.087 | 0 |
| Plant | r1 (m) | 0.612 | 0.612 | 0 |
| | r2 (m) | 1.108 | 1.108 | 0 |
| | r3 (m) | 1.029 | 1.000 | -2.8 |
| | m1 (kg) | 3.155 | 3.155 | 0 |
| | m2 (kg) | 5.892 | 5.892 | 0 |
| | m3 (kg) | 0.900 | 0.079 | -91.2 |
| | μ (kg m2/s) | 0.005 | 0.004 | -20 |
| | I (kg m2) | 11.300 | 10.300 | -8.8 |

The data was analysed for the two critical pressures, the pressure set for the control to initiate and the mean operation pressure. The variation for each parameter between those two pressures was detached in the “Difference” column.

With the previous analysis was finally possible to determine the second order plant coefficients, including the actuator gain, as can be seen in Table 2.

Table 2. Second order plant coefficients.

| | Inicial (Pc = 7bar) | MeOP (Pc = 9.5bar) | Difference (%) |
|---|---|---|---|
| Actuator Gain | 54.038 | 77.233 | 42.9 |
| Plant coef 1 | 1 | 1 | 0 |
| Plant coef 2 | 1.000 | 1.000 | 0 |
| Plant coef 3 | 9.385 | 8.538 | -9.0 |

Using the Sisotool from Matlab an analysis for the system stability was then made for both “Initial” and “MeOP” pressures. The objective of this analysis was to determine gains for a PID controller on which the system had an acceptable stability margin, for both pressures. Figures 9 and 10 gather the Nyquist and Bode plots of the system, as well as the step response, for the “Initial” and “MeOP” respectively.

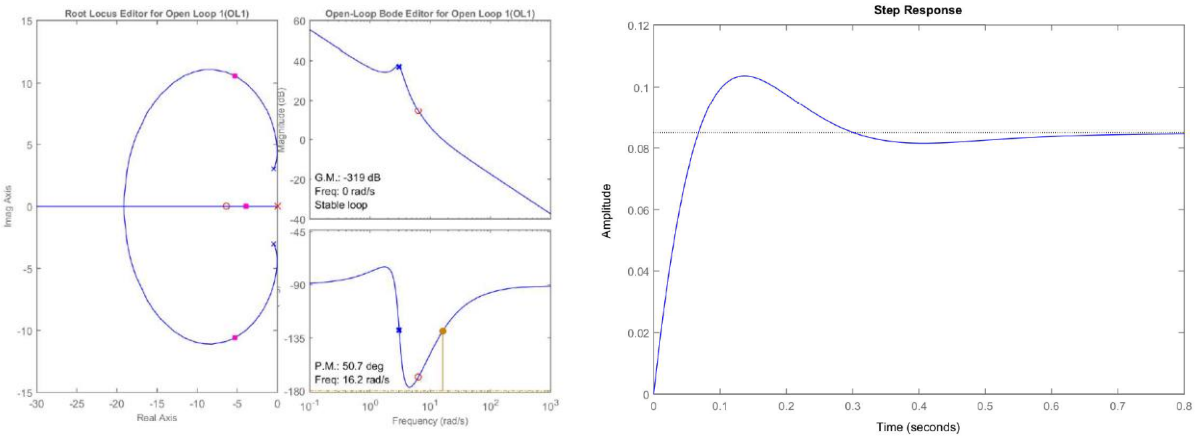


Figure 9. Nyquist plot, Bode plot and step response for the “Initial” control pressure.

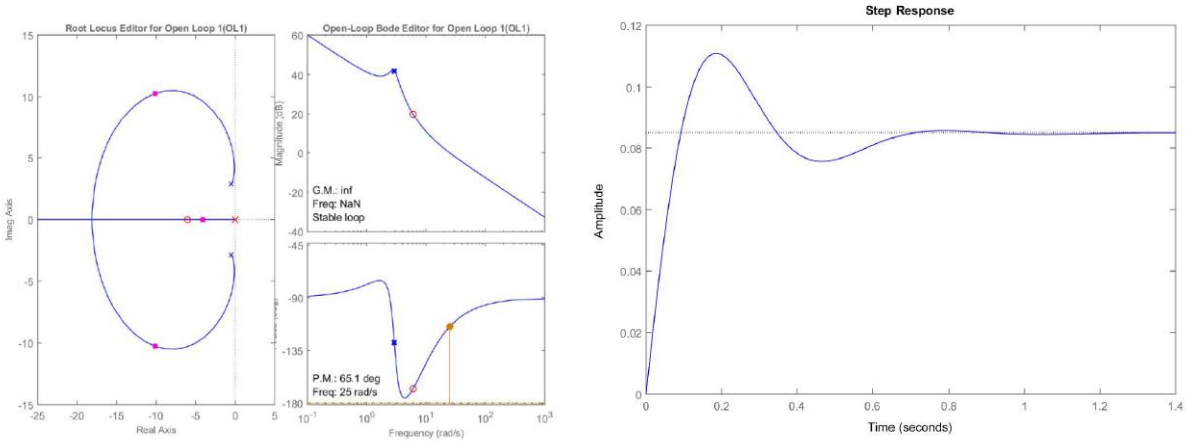


Figure 10. Nyquist plot, Bode plot and step response for the “MeOP” control pressure.

Using the Ziegler-Nichols method in the Sisotool from Matlab, it was finally possible to determine the PID controller gains, shown in Table 3, on which the system would remain with a good margin of stability.

Table 3. Thrust vectoring PID control gains

| | |
|---|---|
| Kp | 3.4 |
| Ki | 10 |
| Kd | 0.3 |

## 4. CONCLUSIONS

A solid rocket motor was designed and fabricated accordingly with a maximum desirable operating pressure using a 0-D chamber pressure model. An extensive experimental work involving hot fire tests was done with the aim of characterizing this solid rocket motor with a high degree of reliability.

With data from chemical equilibrium and drawing softwares as well as from pendulum dynamic tests was possible to calibrate the thrust vectoring control model in order to have an acurate analysis of the PID controller gains.

The propulsive parameters and the controller gains obtained will be fed into the algorithm of the thrust vectoring control system, and then a test phase with the complete mechanism will be performed.

## 5. AKNOWLEDGMENTS

The author is grateful for the support given by CAPES.

## 6. REFERENCES

Anderson, Jr. J.D., 2005. Fundamentals of Aerodynamics, McGraw-Hill, 4th ed.

NASA Chemical Equilibrium with Applications, 2004.

Seidel, H. H., 1965. Transient Chamber Pressure and Thrust in Solid Rocket Motors, Technical Note.

Schaefermeyer, M. R., 2011. Aerodynamic Thrust Vectoring for Attitude Control of a Vertically Thrusting Jet Engine.

Sutton, G. P., 1992. Rocket Propulsion Elements, John Wiley & Sons, 6th ed.

Tewari, A., 2011. Automatic Control of Atmospheric and Space Flight Vehicles, Birkhauser.

Vyverman, T., 1978, The Potassium Nitrate - Sugar Propellant, Report, Belgium.

## 7. RESPONSABILITY NOTICE

The authors are the only responsible for the printed material included in this paper.